Robotica (2025), **43**, pp. 868–886
doi:10.1017/S0263574724002248

CAMBRIDGE UNIVERSITY PRESS

RESEARCH ARTICLE

A simple bipedal robot model demonstrating speed-dependent gait transition

Hirofumi Shin[1] and Shuhei Ikemoto[2,3]

[1]Frontier Robotics, Honda R&D Co. Ltd., Wako-shi, Saitama, Japan
[2]Graduate School of Life Science and Systems Engineering, Kyushu Institute of Technology, Fukuoka, Japan
[3]Research Center for Neuromorphic AI Hardware, Kyushu Institute of Technology, Fukuoka, Japan
Corresponding author: Hirofumi Shin; Email: hirofumi.shin@ieee.org

Received: 1 May 2024; **Revised:** 20 October 2024; **Accepted:** 10 December 2024; **First published online:** 27 January 2025

Keywords: biomimetic robots; bipeds; human biomechanics; robot dynamics; legged robots

Abstract

This paper introduces a novel bipedal robot model designed for adaptive transition between walking and running gaits solely through changes in locomotion speed. The bipedal robot model comprises two sub-components: a mechanical model for the legs that accommodates both walking and running and a continuous state model that does not explicitly switch states. The mechanical model employs a structure combining a linear cylinder with springs, dampers, and stoppers, designed to have mechanistic properties of both the inverted pendulum model used for walking and the spring-loaded inverted pendulum model used for running. The state model utilizes a virtual leg representation to abstractly describe the actual support leg, capable of commonly representing both a double support leg in walking and a single support leg in running. These models enable a simple gait controller to determine the kick force and the foot touchdown point based solely on the parameter of the target speed, thus allowing a robot to walk and run stably. Hence, simulation validation demonstrates the adaptive robot transition to an energy-efficient gait depending on locomotion speed without explicit gait-type instructions and maintaining stable locomotion across a wide range of speeds.

1. Introduction

Transitioning the gait types is an effective strategy for enabling energetically efficient legged locomotion over a wide range of speeds [51]. The gait type is determined by the specific phase relationship of each leg's periodic foot touchdown. For instance, horses exhibit trotting and galloping, while bipeds such as humans demonstrate walking and running [20, 41]. These animals adaptively adjust their gait in response to changes in locomotion speed [50], thereby optimizing energy efficiency during movement [12, 20]. Understanding the gait transition mechanisms in animals is key to achieving adaptive and energy-efficient legged locomotion in robots.

In the field of bipedal robotics, control methods that incorporate gait transitions have been developed. These methods include using different gait pattern generators based on the target gait type [19, 24] and/or adjusting the trajectory or impedance of the reduced-order model according to locomotion speed [26, 45]. Such approaches enable robots to change their gait at arbitrary timings and provide energy-efficient gaits optimized for the locomotion speed. However, unlike animals that adaptively transition their gait in response to locomotion speed, these methods only offer a gait transition policy for environments and robots that closely match the assumed model.

Just as a biomechanics study identified the zero moment point as a criterion for stable human walking [52], which was subsequently utilized in robot walking controllers [23, 49], a method for efficient gait

© The Author(s), 2025. Published by Cambridge University Press.

https://doi.org/10.1017/S0263574724002248 Published online by Cambridge University Press

transition should similarly be inspired by an understanding of the mechanisms of gait transition in animals. In the realm of biomechanics, the mechanism behind human gait transitions [31, 42] is explained using the spring-loaded inverted pendulum (SLIP) model [7, 16]. The efficacy of this model is supported by Geyer et al.'s demonstration that different gaits can be explained using a single model consisting of two SLIP models [16]. Mechanistic properties of human locomotion closely resemble those of the SLIP model, as evidenced by gait observation studies in infants learning to walk unassisted [50]. In contrast, the trajectory of the center of gravity (CoG) increasingly resembles that of the inverted pendulum (IP) model as infants develop independent walking abilities [50]. This acquisition of the IP model is closely related to the development of gait without environmental assistance. Moreover, treadmill experiments with varying speeds confirm that gait transitions occur even with passive changes in locomotion speed [50]. Therefore, the gait transition should be explained as a passive transition between the IP and SLIP models in response to environmental changes.

This paper introduces a novel bipedal robot model that behaves as the IP model during walking and the SLIP model during running. It presents a control method enabling the robot to transition between both gaits suitable for passively varying locomotion speeds. This bipedal robot model, capable of describing both walking and running in a unified manner, is developed by focusing on the similarities in leg states and CoG motions between the two gaits. By utilizing this model, a single gait controller is developed to facilitate both walking and running. Hence, simulation verifications reveal that the gait transitions of a robot occur passively, interacting with the environment without explicit gait-type instructions, and can maintain stable walking and running across a wide range of locomotion speeds. Additionally, these passive gait transitions are shown to be energy-efficient for locomotion over various speeds.

The main contributions of this paper are as follows:

1. Unified Bipedal Robot Model: We propose a novel bipedal robot model that enables adaptive and passive transitions between walking and running gaits, detailed in Section 3. This model integrates a mechanical model for leg dynamics and a continuous state model that governs gait transitions without explicit state switching, offering a unified framework for walking and running.
2. Simple Gait Controller: We develop a single, simple controller based on the bipedal robot model, which can be used for both walking and running, as detailed in Section 4.
3. Stability of Locomotion: We demonstrate the stability of the proposed model through dynamic simulations, showing that stable walking and running are maintained across varying speeds, as detailed in Section 5.2.
4. Passive Gait Transition: Our controller allows for passive gait transitions driven by environmental interactions and changes in locomotion speed, as detailed in Section 5.3.
5. Energy Reduction: By facilitating passive gait transitions, our controller reduces the energy required for locomotion, contributing to more efficient movement across various speeds, as detailed in Section 5.4.

This paper is structured as follows: Section 5.4 introduces relevant studies that underscore the significance of this study and explains the similarities between walking and running. Section 3 proposes a mechanical model that accommodates both walking and running alongside a continuous state model that does not require explicit switching between gait types. Section 4 details the controller developed for the bipedal robot model. The results of the validation are presented and discussed in Section 5. This is followed by a discussion in Section 6, culminating in the conclusions drawn in Section 7.

2. Related work

In this section, we review works related to control methods that facilitate gait changes depending on the locomotion speed. First, the section introduces prior studies on control methods for robots capable of gait transitions, emphasizing the importance of passive gait transitions, and the list of related

https://doi.org/10.1017/S0263574724002248 Published online by Cambridge University Press

Table I. *The list of related works on controllers for gait transitions, explained in Sections 2.1 and 2.2.*

Switching type	Description and references
Controller itself	Switch pattern generator depending on target gait [14, 19, 24] (Section 2.1)
Internal state (CPG)	Switch CPG pattern depending on target gait [25, 40, 48] (Section 2.1)
Internal state (LIP, or SLIP)	Change stiffness of LIP model [18] (Section 2.1), or impedance of SLIP model [26, 27, 31, 37, 42] (Section 2.2), depending on target locomotion speed

works for gait transition controllers is shown in Table I. Then, the focus shifts to the physical model of gait in biomechanics, detailing the characteristics necessary to commonly represent both walking and running.

2.1. Robot controller modification

In humanoid robotics, the controller system often consists of planners and stabilizers, which include inverse dynamics and kinematics calculations. The planner defines the base trajectory for the center of mass [23] and centroidal dynamics [36] and also generates the trajectory for the robot's footstep or contact points. This planner determines the overall gait behavior. The stabilizer corrects the trajectory by compensating for the error between the actual state and the command from the planner trajectory [47] and then outputs the appropriate commands to the robot hardware. Typical control methods based on the linear inverted pendulum (LIP) model employ techniques such as the best COM-ZMP regulator [46] and the divergent component of motion [34, 49] to correct model errors and stabilize the trajectory. These values also provide feedback to the planner for additional balance control [24]. In this controller scheme, the planner part of the controller defines the desired gait behavior. Therefore, we focus on the planner component in the following sections.

In the study of bipedal walking robots, previous control methods, including gait transitions, involve either switching the controller itself [14, 19] and/or altering its internal state [18, 40]. In the switching controller method, specific control rules and pattern generators are prepared for each gait type [14, 24]. An auxiliary controller is implemented to facilitate the switching of the primary controller based on operator input or target speeds, thereby explicitly managing gait transitions. In the altering state method, the controllers are often developed based on a reduced-order model with variable states [18] or a central pattern generator [40]. The former approach enables the CoM to generate vertical motion, which is crucial for both steady-state running and transitions between walking and running, by simply optimizing the stiffness parameter of the liner-inverted pendulum model during each contact phase [18]. The latter approach enables the derivation and adjustment of coordination patterns among the joints in gait motions based on locomotion speed [25]. Altering the coordination pattern in response to the target speed enables adjustments in the locomotion speed of the robot [40], facilitating transitions from walking to running, even though these transitions are discontinuous [48].

These methods force the robot to exhibit locomotion patterns that deviate from its inherent dynamics, potentially resulting in energetically inefficient gaits. A gait transition method that leverages the leg dynamics and does not require explicit gait switching is preferable for more efficient locomotion.

2.2. Leg-model modification

Mechanical models of legs have been extensively studied to abstractly represent the dynamics of walking and running [1, 7, 16, 33]. Based on the characteristics of the CoG motion in human gait,

https://doi.org/10.1017/S0263574724002248 Published online by Cambridge University Press

the IP [11] and the SLIP [7] models are used for the mechanical models for walking and running, respectively. The SLIP model often elucidates the mechanism of transition between these two gait types [7, 13, 16]. This approach is primarily attributed to the work of Gayer et al., who demonstrated that both gaits could be explained using a single model comprising two SLIP models [16], and thereby the model is extended to a variety of control methods [10, 21, 39] and has also been used for bipedal robots [9].

Various control methods that leverage the dynamic properties of mechanical models to enable gait transitions have been developed [26, 27, 31, 37, 42]. Notably, a gait transition in locomotion was effectively demonstrated by using the SLIP model as the mechanical model [43] and adjusting its stiffness [42, 44]. However, the SLIP model alone is insufficient to comprehensively represent the human gait, particularly at slower walking speeds. A lower spring constant is required in lower speed ranges to align the oscillation period of the springs with the walking speed. This results in a significant increase in the amplitude of the CoG, and it is difficult to match walking CoG motion. Therefore, explicit impedance control through a model that integrates the viscosity model is necessary [3, 26, 27, 31].

These models need appropriate parameters (spring and damper constants) for the specific environment. However, the approach might lead to energetically inefficient gaits under environmental conditions different from those anticipated. In other words, methods that rely solely on the SLIP model require explicit modification of leg parameters to fit the expected environment and also require complex compliant legs with variable stiffness [22, 53]. These methods differ in the gait transition mechanism from humans, who adaptively transition their gait in response to environmental changes [50].

2.3. Biomechanics gait description

In biomechanics studies, distinct mechanical models have been traditionally utilized for walking and running [1, 7, 33]. According to analyses of human gait, the SLIP model aptly represents running, while the CoG trajectory during walking exhibits similarities to the IP model as individuals acquire independent walking [50]. Furthermore, because gait transitions can also occur due to changes in locomotion speed caused by external factors [50], it is desirable to explain these transitions through passive changes in these different mechanical models.

In studies that use different mechanical models for running and walking, the focus is often on the behavior of the legs during their dominant phases. Running of the single support phase is typically represented by the SLIP model [7, 17], while walking of the single support phase is described by the IP model [1, 6]. However, these gaits exhibit distinct behaviors in each phase, even with the same gait type. Running alternates between a flight (F) phase and a single support (SS_{run}) phase, represented as an inelastic leg (constant acceleration motion) and an elastic leg (SLIP model), respectively [7]. Walking involves a single support (SS_{walk}) phase and a double support (DS) phase, which are described by a rigid leg (IP model) and elastic legs (SLIP model) [29, 30]. Despite the similarity in the single support phase (SS_{walk} and SS_{run}), the difference in the order of contact (F $\rightarrow$ SS or DS $\rightarrow$ SS) and the resulting varied state of leg elasticity (SLIP and IP models) make it difficult to explain gait transitions solely through passive behavior of models.

On the other hand, by focusing on CoG motion rather than the behavior of the legs themselves, walking and running show similarities in the shape of their trajectories. The CoG motions in both gaits oscillate upward and downward once in each gait cycle, resembling the motion of a bouncing rubber ball [8]. The CoG trajectory during the SS_{run} and DS phases is lower convex, while the trajectory is upper convex during the F and SS_{walk} phases. The legs compress and extend in a manner akin to the elastic leg (SLIP model) during the lower convex trajectory [29, 30], and they behave as inelastic legs, not undergoing compression or extension during the upper convex trajectory. Thus, walking and running can be commonly described as alternating between leg elastic states during the lower convex trajectory and inelastic states during the upper convex trajectory.

https://doi.org/10.1017/S0263574724002248 Published online by Cambridge University Press

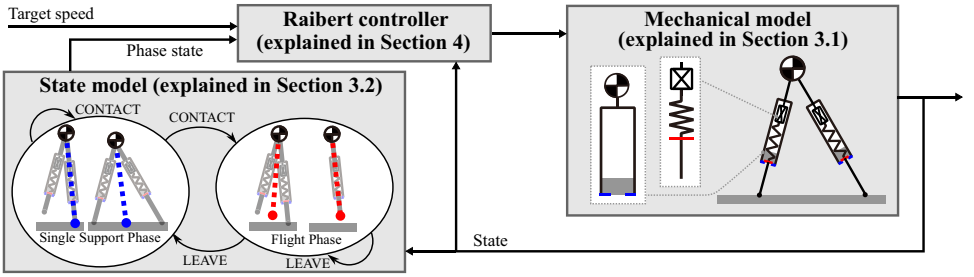


Figure 1. *The overall structure of the proposed controller for speed-dependent gait transition. The controller consists of the bipedal model (mechanical model and state model) explained in Section 3, along with the Raibert controller explained in Section 4.*

These variations in the CoG motion are due to its interactions with external forces, including environmental influences. Developing a mechanical model in which the mechanistic properties of the leg passively change in response to external forces can provide a way to explain gait transitions as passive phenomena. This study focuses on the CoG motion and proposes a mechanical model capable of representing both the IP and SLIP models, along with a state model whose state representations do not depend on gait types. Utilizing these models, we aim to develop a bipedal robot model that adaptively transitions between walking and running depending on locomotion speed.

3. Methodology

This section presents a biped robot model capable of adaptive gait transitions. The overall structure is shown in Figure 1. The model is constructed from the following two sub-models:

(a) **Mechanical Model** alternates its mechanistic properties between the IP model (inelastic leg) and the SLIP model (elastic leg), depending on the external force and/or ground reaction force,

(b) **State Model** commonly represents the state transitions between walking and running without explicit state switching based on the gait type.

3.1. Mechanical model

In order to enable passive gait transitions in response to changes in locomotion speed, it is necessary to have a mechanical model for the leg that can switch between inelastic and elastic states depending on external forces and/or ground reaction forces is necessary. Therefore, we propose a novel mechanical model, illustrated in Figure 2, which consists of a cylinder, spring, and damper.

This mechanical model comprises a cylinder part and a shaft part. The lower portion of the cylinder part includes a stopper and a damper part. An actuator, spring, and stopper are connected in series within the shaft part. These two stoppers either make contact or separate. Let the CoM position as $\boldsymbol{p}_c = [x_c, y_c]^T$, the equation of motion (EoM) for this mechanical model is expressed as follows:

$$m\ddot{\boldsymbol{p}}_c = \boldsymbol{f}_m + mg[1, 0]^T, \tag{1a}$$

$$\boldsymbol{f}_m = K(\boldsymbol{p}_c, l_a) - C(\dot{\boldsymbol{p}}_c, \boldsymbol{p}_c), \tag{1b}$$

where m and g represent the mass and gravitational acceleration, respectively, and variables and constants frequently mentioned in subsequent sections are listed in Table II. In order to vary the leg properties affected by the stopper, damper, and spring in response to external forces, the spring force $K(\boldsymbol{p}_c, l_a)$ and damper force $C(\dot{\boldsymbol{p}}_c, \boldsymbol{p}_c)$ are defined in the same manner with Geyer's SLIP model [16] as follows:

https://doi.org/10.1017/S0263574724002248 Published online by Cambridge University Press

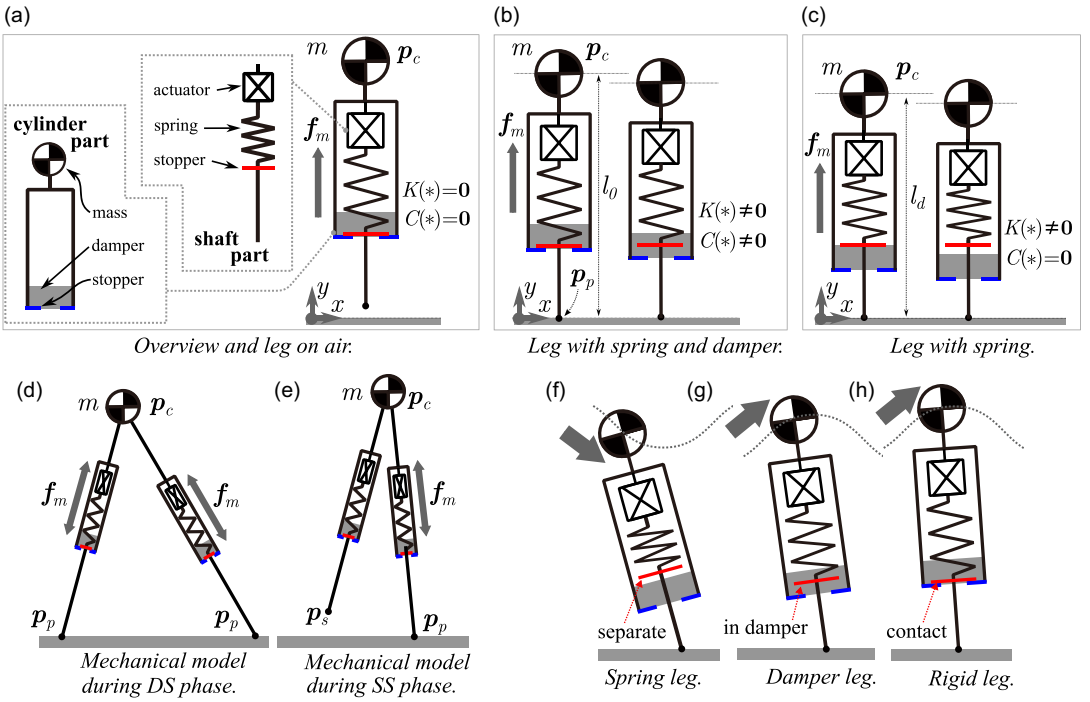


Figure 2. *Overview of the spring-loaded inverted pendulum model with a cylinder to replicate the behaviors of both SLIP and IP models. Panel (a) illustrates the structural details with the leg in the air. Panels (a) to (c) show how the spring and damper forces are generated depending on the leg length. $K(*)=\mathbf{0}$ and $K(*)\neq\mathbf{0}$ correspond to the lower case and upper case of (2), respectively. Similarly, $C(*)=\mathbf{0}$ and $C(*)\neq\mathbf{0}$ represent the lower and upper cases of (3). Panels (d) and (e) indicate how the mechanical model is structured during the DS and SS phases. Panels (f) to (h) display the changes in the mechanical properties of the leg model depending on leg behaviors.*

$$K(\boldsymbol{p}_c, l_a) = \begin{cases} k_0 \left(\frac{l_0 + l_a}{|\hat{\boldsymbol{p}}_c|} - 1 \right) \hat{\boldsymbol{p}}_c, & \text{if } |\hat{\boldsymbol{p}}_c| < l_0 \,; \\ \mathbf{0}, & \text{otherwise} \,, \end{cases} \tag{2}$$

$$C(\dot{\boldsymbol{p}}_c, \boldsymbol{p}_c) = \begin{cases} c_0 \frac{\hat{\boldsymbol{p}}_c^T \dot{\boldsymbol{p}}_c}{|\hat{\boldsymbol{p}}_c|^2} \hat{\boldsymbol{p}}_c, & \text{if } l_d < |\hat{\boldsymbol{p}}_c| < l_0 \,; \\ \mathbf{0}, & \text{otherwise} \,, \end{cases} \tag{3}$$

where,

$$\hat{\boldsymbol{p}}_c = \boldsymbol{p}_c - \boldsymbol{p}_p. \tag{4}$$

k_0 and c_0 are the spring and damper constants, respectively. Here, $\hat{\boldsymbol{p}}_c$ denotes the CoM position with $\boldsymbol{p}_p$ as the origin. Define l_0 as the natural length of the spring and l_a as the length of the actuator, which indicates the forced displacement from the natural length. When both stoppers are in contact, the leg reaches its maximum length l_0, as illustrated in the left figure of Figure 2(b). As the leg shortens from this maximum length, the stopper initially traverses through the damper region, as shown in the right figure of panel (b), during which both the damper and the spring generate forces. At even shorter lengths, the stopper enters the non-damper region, as illustrated in the right figure of panel (c), during which force is generated only by the spring. Here, let l_d be the leg length at the boundary between the damper and non-damper regions. Note that let $\boldsymbol{p}_p$ represent the foot contact position with the ground, and its velocity

https://doi.org/10.1017/S0263574724002248 Published online by Cambridge University Press

Table II. *List of variables and parameters. Each position is a two-dimensional vector as* $\boldsymbol{p}_* = [x_*, y_*]$.

Type	Var.	Description
Position	$\boldsymbol{p}_c$	Center of mass (CoM)
Foot position	$\boldsymbol{p}_p$	Actual support leg
	$\boldsymbol{p}_{p,i}$	Multiple support legs
	$\boldsymbol{p}_s$	Actual swing leg
	$\boldsymbol{p}_{vp}$	Virtual support leg
	$\boldsymbol{p}_{vs}$	Virtual swing leg
Force	$\boldsymbol{f}_m$	Given by leg model
Superscript	X^d	Command value for X
	X^{d*}	Target value for X
Physical	m	Mass
	k_0	Spring constant
	c_0	Damping constant
Length	l_0	Max mechanical model
	l_d	Dempper affected
	l_a	Actuator input
Gain	c_{fp}	Velocity P control
	c_{kp}	Height P control
	c_{ki}	Height I control

is specified to describe the foot lift-off from the ground as described as

$$\dot{\boldsymbol{p}}_p = \begin{cases} \boldsymbol{0}, & \text{if } |\hat{\boldsymbol{p}}_c| < l_0\,; \\ \dot{\boldsymbol{p}}_c, & \text{otherwise}\,. \end{cases} \tag{5}$$

The EoM from (1a) to (5) represents the mechanical model for a single leg. In order to construct a mechanical model for a biped, the forces f_m from both legs need to be added to (1a). Therefore, during the DS phase, each leg is assigned its own leg variables, and both legs independently generate their respective forces f_m from (1b), as shown in Figure 2(d). During the SS phase, the single force f_m from (1b) is added to (1a), as shown in Figure 2(e).

The mechanistic properties of this model change depending on the external and ground reaction forces applied to the CoM. As depicted in Figure 2(f), when an external force induces a lower convex trajectory of the CoM, the model behaves as an elastic leg (SLIP model) with only the spring action. Conversely, when an external force leads to an upper convex trajectory of the CoM, the model initially behaves as an inelastic leg, predominantly influenced by the damper, as shown in Figure 2(g). Subsequently, the model turns into an inelastic leg (IP model or foot lift-off) where neither the damper nor the spring has an effect, as illustrated in Figure 2(h). Here, note that in the situation of Figure 2(g), the spring action becomes non-dominant in some cases on the damper parameters. Thus, this mechanical model enables a passive transition between elastic legs (SLIP model) and inelastic legs (IP model, flying), depending on the applied external force.

3.2. State model

A state model that does not differentiate between walking and running is needed for passive adaptation of the gait to suit various environmental conditions, such as external forces, ground reaction forces, and locomotion speed. The state model consists of leg representations and a state machine. In this study, we

https://doi.org/10.1017/S0263574724002248 Published online by Cambridge University Press

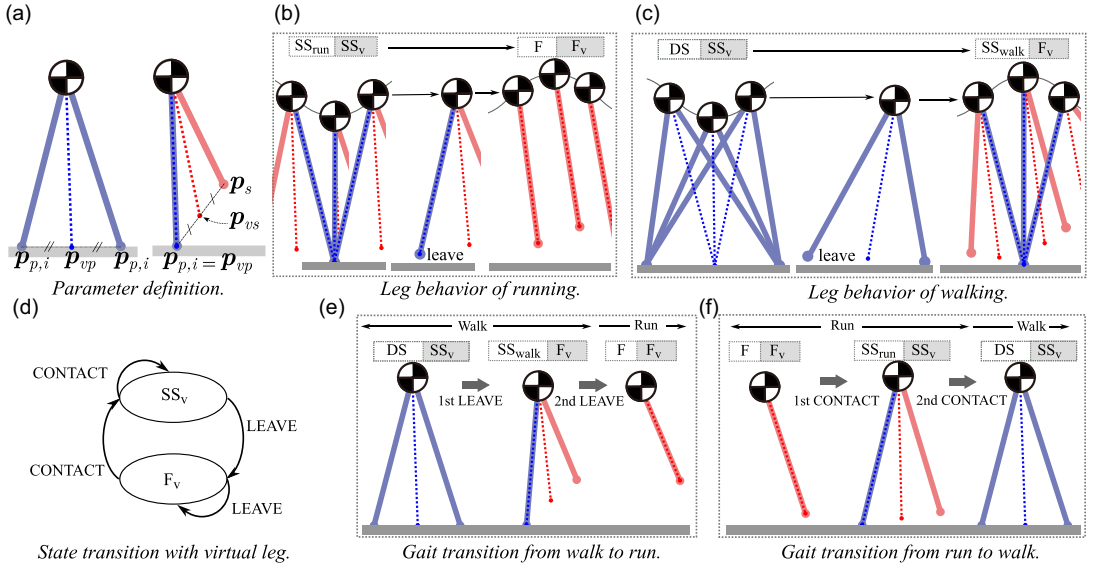


Figure 3. *State model for unified gait transition during walking and running. The blue and red lines represent the supporting and swinging legs, respectively. The dashed blue and red lines denote the virtual supporting leg and the virtual swinging leg. The white and gray boxes above the panels indicate the actual gait and virtual leg phases, respectively. Panel (a) illustrates the parameter definitions for the virtual leg description. Panels (b) and (c) depict leg behaviors with virtual legs. Panel (d) presents the state transition diagram. Panels (e) and (f) display leg behaviors during gait transitions.*

introduce a state model based on leg representations common to both walking and running, and a state machine developed from these representations.

By introducing virtual leg representations, we develop a unified approach to leg representation applicable to both walking and running. These virtual legs consist of a virtual support leg and a virtual swing leg. As depicted in Figure 3(a), the foot positions of these legs are defined as $\boldsymbol{p}_{vp}$ for the virtual support leg and $\boldsymbol{p}_{vs}$ for the virtual swing leg. The virtual support leg $\boldsymbol{p}_{vp}$ is the midpoint among all actual support legs, while the virtual swing leg $\boldsymbol{p}_{vs}$ is the midpoint between the actual swing leg and $\boldsymbol{p}_{vp}$. Accordingly, the foot position of the virtual support and swing legs are obtained as follows:

$$\boldsymbol{p}_{vp} = \frac{1}{|L_p|} \sum_{i \in L_p} \boldsymbol{p}_{p,i}, \tag{6}$$

$$\boldsymbol{p}_{vs} = \frac{1}{2}(\boldsymbol{p}_s + \boldsymbol{p}_{vp}), \tag{7}$$

where L_p signifies the set of all actual support legs, and $|L_p|$ represents the number of support legs. Therefore, (6) shows the midpoint of all support legs as depicted in Figure 3(a). Define $\boldsymbol{p}_{p,i}$ as an extension variable of the foot position of the actual support leg $\boldsymbol{p}_p$ to accommodate multiple legs. These variables are recalculated upon the occurrence of a LEAVE and CONTACT event, which will be defined subsequently, as follows:

Actual Support Leg: when y-coordinate of $\boldsymbol{p}_s$ is lower equal than zero, $\boldsymbol{p}_s$ is reallocated as $\boldsymbol{p}_{p,i}$
Actual Swing Leg: when y-coordinate of $\boldsymbol{p}_{p,i}$ is larger equal than zero, $\boldsymbol{p}_{p,i}$ is reallocated as $\boldsymbol{p}_s$.

Using these foot positions of actual support leg $\boldsymbol{p}_{p,i}$ and actual swing leg $\boldsymbol{p}_s$, the virtual legs (6) and (7) are obtained. Note that the controller, which will be detailed in Section 4, adjusts the position of the virtual swing leg $\boldsymbol{p}_{vs}$, and then this position dictates the position of the actual swing leg, $\boldsymbol{p}_s$.

https://doi.org/10.1017/S0263574724002248 Published online by Cambridge University Press

Utilizing this virtual leg representation allows for the four phases of walking and running (DS, SS_{run}, SS_{walk}, and F) to be represented as two phases of virtual legs (SS_v and F_v). As shown in Figure 3(b)(c), the virtual support leg during the DS and SS_{run} phases exhibit behavior similar to that of the SS_{run} phase in the running, as indicated by the blue dashed line. Likewise, the virtual swing leg during the SS_{walk} and F phases mirror the behavior of the F phase in the running, as denoted by the red dashed line. Therefore, the DS and SS_{run} phases enable to be represented as the SS_v phase of the virtual leg, whereas the SS_{walk} and F phases can be represented as the F_v phase of the virtual leg.

Using the virtual legs, the description of walking and running within a single state machine is shown in Figure 3(d). The state machine consists of event conditions and transition rules, while the virtual leg representation provides simple event conditions and transition rules for gait. The event condition is defined to determine whether the virtual leg touchdowns or lift-off from the ground, as follows:

LEAVE: when the foot position of current virtual support is $y_{vp} > 0$,
CONTACT: when the foot position of current virtual swing leg is $y_{vs} \leq 0$, and the current CoM velocity is $\dot{y}_c \leq 0$.

Here, given that the relationship between the virtual leg and the actual leg is defined through equations (6) and (7), LEAVE corresponds to the lift-off of any actual leg, while CONTACT corresponds to the touchdown of any actual leg. The transition rules are based on the LEAVE and CONTACT events of the virtual legs as follows:

Rule1: when previous event is LEAVE, phase becomes F_v,
Rule2: when previous event is CONTACT, phase becomes SS_v.

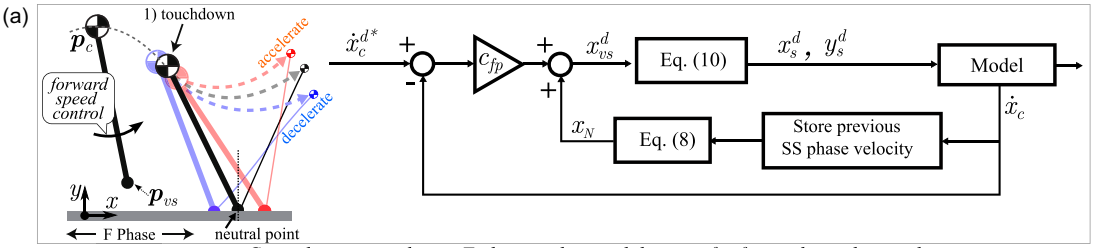
Only employing this state machine with these simple event conditions and transition rules provides an explanation of the walking and running, including their transition.

First, the leg behaviors of each state transition for walking and running are illustrated in Figure 3(b) and (c), respectively. The walking alternates the DS and SS_{walk} phases, whereas the running repeats the SS_{run} and F phases. In the virtual leg representation, both gaits alternate between the SS_v and F_v phases. In other words, the same gait pattern is maintained as long as the CONTACT and LEAVE events (or the SS_v and F_v phases) occur in alternation. Next, the leg behaviors during gait transitions are shown in Figure 3(e) and (f). Figure 3(e) illustrates the gait transition sequence from walking to running occurs through "DS $\rightarrow$ SS_{walk} $\rightarrow$ F." During these phase transitions, the virtual leg transitions from the SS_v phase to the F_v phase following the initial LEAVE event. Subsequently, the position of the virtual support leg is recalculated, as indicated by the blue dashed line in the central diagram, which triggers a second successive LEAVE event. Similarly, two successive CONTACT events from the F_v phase facilitate the transition from running to walking, as depicted in Figure 3(f). Thus, gait transitions arise when the sequence of alternating CONTACT and LEAVE events (or transitions between the SS_v and F_v phases) is discontinued. Furthermore, these transitions are hypothesized to occur when there is excessive energy (in terms of walking speed) relative to the current gait.

The state model does not retain specific information to distinguish between walking and running while enabling it to describe the state transitions for both gait types without distinction of their types. Furthermore, it is assumed that the irregularities in events leading to gait transitions, such as the successive occurrences of CONTACT or LEAVE, arise passively due to changes in the interaction between the robot and the ground depending on the changes in locomotion speed.

The bipedal robot model, comprised of both the mechanical and state models, commonly enables the representation of the robot's model, regardless of whether the legs function as rigid or spring legs, regardless of whether the current gait type is walking or running. The method has the possibility to autonomously select the gait type depending on the interaction between the environment and the robot. In the subsequent section, a method to control the locomotion speed of this bipedal robot model will be introduced, and this behavior will be verified in dynamics simulations.

https://doi.org/10.1017/S0263574724002248 Published online by Cambridge University Press



Control overview during F phase and control diagram for forward speed control.

Control overview during SS phase and control diagram for jump height control.

Figure 4. *Phase definition and control diagrams in Raibert controller [38], which consists of compression, trust phase, and touchdown period. The parameter definitions are in Tables II and III.*

4. Implementation of controller

Owing to the similarity in behavior of the proposed virtual legs to running, the control method developed by Raibert et al., often used in running control [15, 38], is implemented in the controller for our bipedal robot model. The control system treats jump height, forward speed, and body attitude as separate control problems, as illustrated in Figure 4. First, applying leg kick force during the thrust phase adjusts the peak jump height in the F phase. This kick force compensates for the energy dissipated through the impact at foot touchdown and the viscoelastic properties of the leg during the compression phase. Second, body attitude control working during the SS phase maintains the robot's upper body posture upright during running. Last, the forward speed is adjusted by foot placement at the touchdown, which is the foot touchdown point at the end of the F phase. The foot touchdown at the neutral point, which is the position where the motion of the support leg is symmetrical during the SS phase (indicated by the gray dotted line in the figure), maintains forward speed. When the foot contacts forward or backward from the neutral point, the motion of the support leg becomes asymmetrical (indicated by the red and blue dotted lines in the figure), thereby accelerating or decelerating the forward speed of the robot. Note that this control method is based on the assumption of minimal inertia effects in the legs; this feature is often mirrored in actual robots with designs where the mass is concentrated near the CoM position. Consequently, it is premised that variations in the touchdown point do not affect the behavior during the previous F phase.

Raibert's control framework allows continuous running with three independently executed control algorithms. In this study, we selectively use the forward speed control and the jump height control from Raibert's controller to control the running behavior of the virtual leg.

4.1. Forward speed control

The foot touchdown point is determined by adding a positional correction for acceleration or deceleration (p control correction) to the neutral point, which keeps forward speed [38]. This correction to the foot touchdown point is directly applied to determine the foot point of the virtual swing leg, as detailed in (7). Let the duration and average velocity of the previous SS phase as T_{PS} and $\dot{x}_{PS}$, respectively [38], the neutral point is obtained as follows:

https://doi.org/10.1017/S0263574724002248 Published online by Cambridge University Press

$$x_N = \frac{\dot{x}_{PS} T_{PS}}{2}, \tag{8}$$

where, for simplicity in this study, $\dot{x}_{PS}$ is taken as the velocity $\dot{x}_c$ at midstance during the previous SS_v phase. Note that because the neutral point is dynamically adjusted by the duration (T_{PS}) of the previous SS phase, the neutral point can vary even at the same velocity. The touchdown point of the virtual swing leg touchdown is calculated by adding the neutral point and the p control term, which is determined as follows:

$$x_{vs}^d = x_N + c_{fp}(\dot{x}_c^{d*} - \dot{x}_c), \tag{9}$$

where c_{fp} is a constant, and $d*$ and d, denote the target and control command values, respectively. The point of the actual swing leg is obtained by the relationship between (9) and (7) as follows:

$$\begin{bmatrix} x_s^d \\ y_s^d \end{bmatrix} = \begin{bmatrix} 2(x_{vs}^d - x_{vp}) + x_{vp} \\ y_c - \sqrt{l_0^2 - \left(x_s^d\right)^2} \end{bmatrix}, \tag{10}$$

where the position is determined by the target locomotion speed $\dot{x}_c^{d*}$. The control diagram for forward speed control is shown on the right side of Figure 4(a).

4.2. Jump height control

The kick force of the leg is determined by its energy, calculated as the difference between the target energy E^{d*}, based on the desired jump height, and the current energy E. Let the target maximum height be defined as y_c^{d*}, the target energy E^{d*} is obtained according to:

$$E^d = mgy_c^{d*} + \frac{1}{2}m\left(\dot{x}_c^{d*}\right)^2. \tag{11}$$

The current energy is obtained as follows:

$$E = mgy_c + \frac{1}{2}m\dot{\boldsymbol{p}}_c \cdot \dot{\boldsymbol{p}}_c + \frac{1}{2}\frac{\left(K(\boldsymbol{p}_c, l_a)\right)^2}{k_0}, \tag{12}$$

where the kick force of our mechanical model results from the forced displacement of the spring l_a. Consequently, the kick force is defined through PI control with the forced displacement l_a as the control input and energy as the control output, as follows:

$$l_a = c_{kp}e + c_{ki}\int e dt, \tag{13}$$

$$e = E^{d*} - E, \tag{14}$$

where c_{kp} and c_{ki} represent the p and I gains, respectively. Note that to provide positive energy, the kick force is generated by legs positioned behind the CoM on the x-axis. The control diagram for jump height control is shown on the right side of Figure 4(b).

5. Verification

This section shows that the developed bipedal robot model, in conjunction with the previously explained control method, demonstrates the gait transitions of the robot both passively and adaptively. Through dynamic simulations, the stability of the bipedal robot model was demonstrated, and the behavior of the model, along with the dynamics of energy change during the transition, was verified under gradual changes in locomotion speed.

https://doi.org/10.1017/S0263574724002248 Published online by Cambridge University Press

Table III. *List of parameters for the simulation verifications.*

Param.	Value
m	80.0kg
k_0	50000 N/m
c_0	1000 Ns/m
l_0	1.00m
l_d	0.95 m
c_{fp}	0.1
c_{kp}	1.0×10^{-4}
c_{ki}	1.0×10^{-7}

5.1. Setup for simulation

Dynamics simulations were carried out by numerically integrating the EoM from (1a) to (5) using the Euler method. The simulation parameters are specified in Table III. Two simulation scenarios were established. In the first scenario, independent simulations were performed for each target velocity to analyze stability. The target locomotion speeds $\dot{x}_c^{d*}$ ranged from 0.5 m/s to 3.0 m/s, with increments of 0.01 m/s between each simulation. Each trial was executed over a duration of 50 seconds at the specified target velocity. The second scenario involved increasing or decreasing the target locomotion speed during a continuous simulation to demonstrate gait transitions. The initial velocity was set at $\dot{\boldsymbol{p}}_c = [0.5, 0.0]^T$ and gradually increased from 0.5 m/s to 3.0 m/s by 0.01 m/s every 2 seconds. Conversely, another simulation began at $\dot{\boldsymbol{p}}_c = [3.0, 0.0]^T$, where the target locomotion speed was decreased from 3.0 m/s to 0.5 m/s. The initial position and target height for both simulations were set to $\boldsymbol{p}_c = [0, 1.02]^T$ and $y_c^{d*} = 0.99$ m, respectively.

5.2. Results of stability analysis

The results of the first scenario are shown in Figure 5. The larger dots represent the result from the first half of the simulation, while the smaller dots represent the results from the second half. These dots illustrate the deviation between the velocity when the CoM reaches peak height position during the previous and current SSv phases, a type of Poincaré section. When this deviation converges to zero, it indicates asymptotic stability. Conversely, when the deviation remains within a certain range, it indicates marginal stability. In most of the simulation results, the system exhibits asymptotic stability, as indicated by the convergence of the velocity deviations to zero. However, at around 1.3 m/s and 2.0 m/s, the system does not exhibit asymptotic stability; rather, it demonstrates marginal stability. This is indicated by the clusters of smaller purple dots positioned between the clusters of larger dots, meaning that the velocity deviations remain bounded within a certain range rather than converging to zero. Note that the regions where asymptotic stability does not show correspond to areas where gait transitions occur, which will be explained in detail in the next section. These regions exhibit marginal stability rather than asymptotic stability.tm

Additionally, in the low-speed range (below 1.8 m/s), the leg behavior corresponds to walking, characterized by alternating DS and SS_{walk} phases, as shown in Figure 6(a). Conversely, in the high-speed range (above 1.9 m/s), the leg demonstrates running behavior, repeating F and SS_{run} phases, as shown in Figure 6(b). These results demonstrate that our bipedal robot model can achieve stable locomotion over a wide range of speeds, with the appropriate gait being automatically selected based on the speed.

5.3. Results of gait transition behavior

The results of the second scenario are shown in Figure 7. Panels (a) and (b) show simulation results that depict changes in the CoM velocity to verify passive gait transitions. The thin blue line of the figure is the

https://doi.org/10.1017/S0263574724002248 Published online by Cambridge University Press

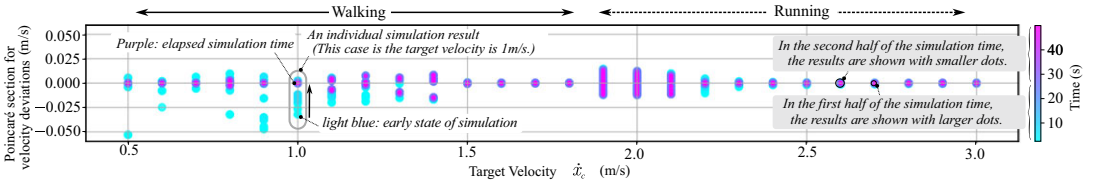


Figure 5. *Result of the Poincaré section for velocity deviations for each individual target velocity. Each dot represents the velocity deviation between the current and previous phases, where the speed is measured when the CoM reaches peak height position.*

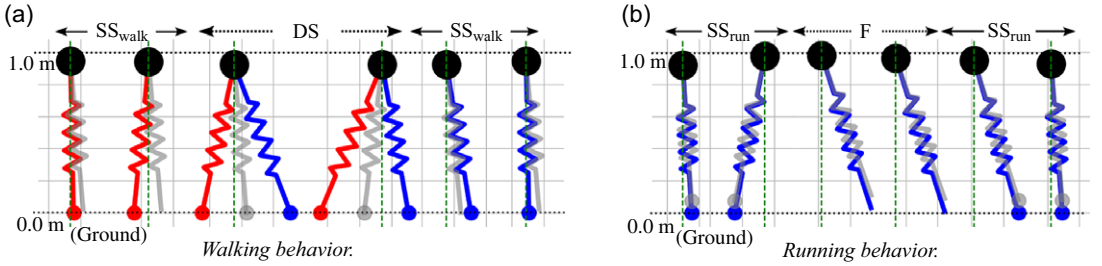


Figure 6. *Leg behavior in simulation. The red and blue legs show the actual legs, which are the left and right feet. The gray shows the virtual legs. While the legs come in contact with the ground, round markers at the tip of the legs are shown. Panel (a) shows a walking motion. Panel (b) shows a running motion.*

CoM velocity $\dot{\boldsymbol{p}}_c$. The bold blue line illustrates $\dot{\boldsymbol{p}}_c$ at certain target speeds; the bold blue line represents walking, while the bold red line represents running. Panels (c) to (f) show the phase transitions for both the virtual and actual legs to provide insight into how the gait transitions occur. The gray lines represent the phases of the virtual legs, while the black lines depict the resulting phases of the actual legs.

First, the walking pattern is depicted as the bold blue line in Figure 7, which shows trapezoidal limit cycle trajectories. During walking, the phases of the virtual legs alternate between the SS_v and F_v phases, while the phases of the actual legs alternate between the DS and SS_{walk} phases, as shown in Figure 7(c). This pattern aligns with the explanation provided in Figure 3(c).

Second, the running pattern is depicted as the bold red line in Figure 7, which shows a semicircular limit cycle trajectory. During running, the phases of the virtual legs alternate between the F_v and SS_v phases, while the phases of the actual legs alternate between the F and SS_{run} phases, as shown in Figure 7(e). This pattern also aligns with the explanation provided in Figure 3(b).

Third, the walk-to-run transition behavior is shown in the delineated gray region of Figure 7(a), with phase transitions illustrated in Figure 7(d). At the beginning of the gait transition, the phase of the virtual legs transitions from SS_v to F_v, while the phase of the actual legs transitions from DS to SS_{walk}. At that moment, the virtual stance leg is recalculated by (6) and is placed in the same position as the current actual stance leg. Next, when both the virtual and actual stance legs leave the ground, the phase of the actual legs transitions from SS_{walk} to F, while the phase of the virtual legs remains in the F_v phase. Consequently, the gait phase transitions to running. This pattern also aligns with the explanation provided in Figure 3(e).

Lastly, the run-to-walk transition behavior is shown in the delineated gray region of Figure 7(b), with phase transitions illustrated in Figure 7(f). At the beginning of the gait transition, the phase of the virtual legs transitions from F_v to SS_v, while the phase of the actual legs transitions from F to SS_{run}. At that moment, the virtual swing leg is recalculated by (7), while the actual swing leg is redefined by (10). Next, when the actual swing leg contacts the ground, the phase of the actual legs transitions from SS_{run}

https://doi.org/10.1017/S0263574724002248 Published online by Cambridge University Press

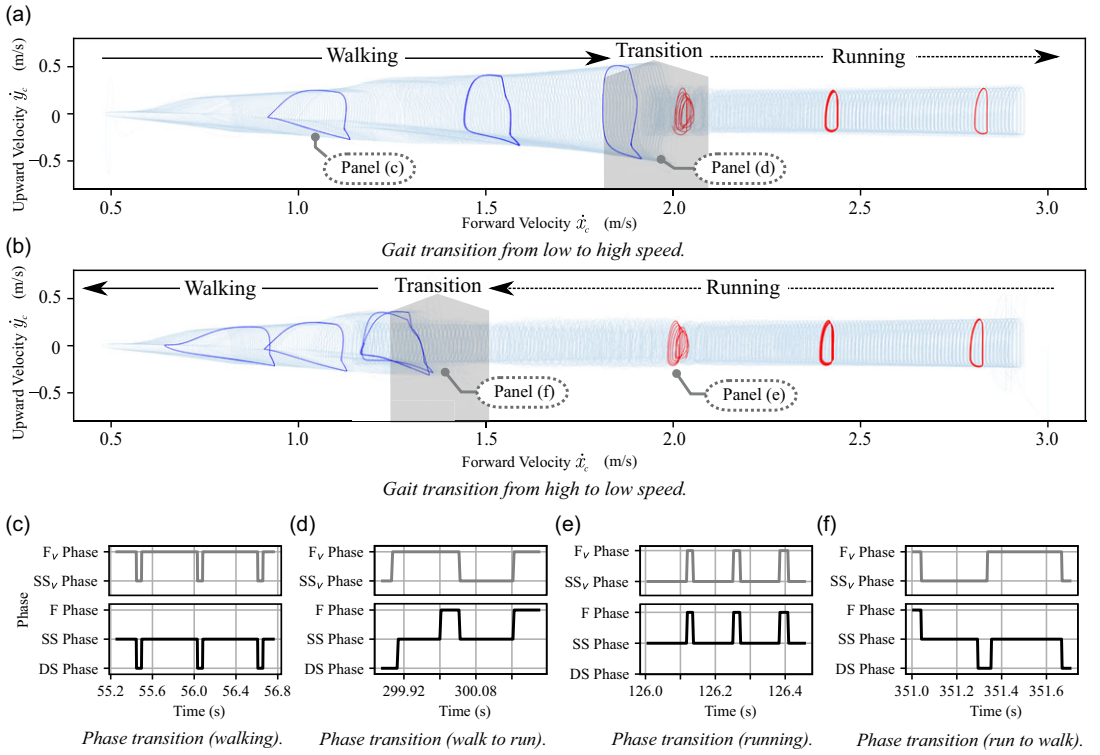


Figure 7. *Phase diagrams during the target speed are changed discontinuously during a continuous simulation. The target speed of panel (a) is changed from* 0.5 *m/s to* 3.0 *m/s every* 0.01 *m/s, and it of panel (b) is the reverse. Although the result of decreasing and increasing speed has hysteresis, this graph shows stable motion in any speed range. Panels (c) to (f) show the actual phase transitions for the virtual leg and the actual leg, with their timings illustrated in panels (a) and (b), respectively.*

to DS, while the phase of virtual legs remains in the SS_v phase. Consequently, the gait phase transitions to walking. This pattern also aligns with the explanation provided in Figure 3(d).

These graphs show hysteresis existing in the speeds at which gait transitions occur. These regions, where the robot exhibits marginal rather than asymptotic stability in the stability analysis (as shown in Figure 5), are closer to the areas where gait transitions occur, as indicated in Figure 6. During the speed increase from low to high depicted in Figure 6(a), the gait transition is observed at approximately 2.0 m/s. Conversely, during the speed decrease from high to low, as shown in Figure 6(b), the gait transition occurs at around 1.4 m/s. While these results indicate the presence of hysteresis and some regions of non-asymptotic stability, the system in all regions exhibits either asymptotic or marginal stability. These results indicate that the gait transitions of the robot occur passively, triggered by the interaction between the robot and the environment in response to changes in locomotion speed, and that a stable gait can be maintained across a broad spectrum of speeds.

5.4. Result of input energy

To verify that an adaptively efficient gait is selected, the energy consumed during the simulations of the second scenario was calculated, and the results are shown in Figure 8. The total energy input from the kick force (jump height control) at each target speed is plotted as gray dots. The cubic curve approximation of these points is represented by bold lines (red and blue), with the blue line indicating the walking and the red line indicating the running state.

https://doi.org/10.1017/S0263574724002248 Published online by Cambridge University Press

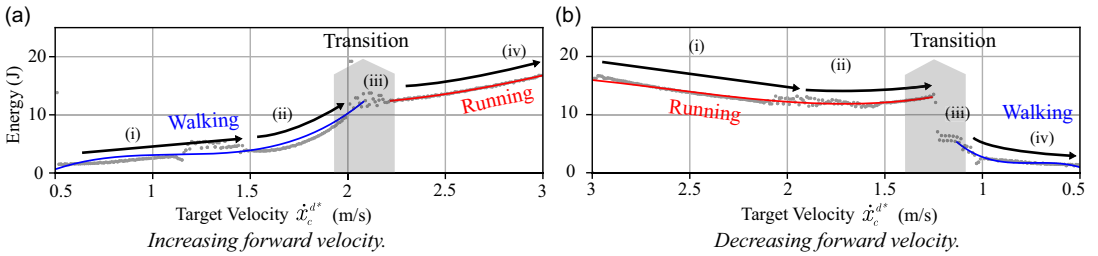


Figure 8. *Change in energy as a function of target velocity. Panel (a) shows the change from low to high speed, and panel (b) shows the reverse.*

The input energy for the transition from low to high speed is depicted in Figure 8(a), with the transition phases marked as (i)∼(iv). Initially, in (i), the robot begins walking, with input energy monotonically increasing alongside locomotion speed. Upon further velocity increase, (ii) exhibits a sharp escalation in input energy, yet the robot continues to walk. Continuing to increase the speed led to a significant change in the rate of energy increase in (iii), transitioning to a running gait. Subsequently, in (iv), the energy monotonically increased at a rate smaller than in (ii). These changes of energy are also shown in the transition from high to low speeds, shown in panel (b), through the speed range for (iii).

Hence, as the target speed increases (decreases), the energy consumption for gait correspondingly increases (decreases). Fundamentally, these results showed gradual energy changes, as illustrated in phases (i) and (iv) in Figure 8. On the other hand, as the locomotion speed closes to the speed range for gait transition, indicated by the gray area, a significant amount of energy is needed, exceeding these gradual changes (i) and (iv). In other words, the results indicate that an excess of energy is required before the gait transition occurs, and the transitioning gait makes the robot reduce the needed energy.

In summary, our proposed bipedal robot model has demonstrated passive gait transitions through modifications in locomotion speed. Furthermore, it has been confirmed that the process of gait transition contributes to a reduction in the energy necessary for locomotion across the respective speed range, thereby enhancing energy efficiency.

6. Discussion

The results indicated that our method passively transitioned from walking to running gait and vice versa using the same stiffness (mechanical model), a single state transition rule, and a single controller without explicit controller switching. Similar gait transition controllers based on the spring-mass model, on the other hand, explicitly change the impedance of a damper-added SLIP model [26] or discontinuously adjust the stiffness of the SLIP model, even though they use a unified mechanical model for both walking and running [42]. These controllers, which explicitly change internal states [26, 42], require a significant increase in energy during the transition from walking to running. In contrast, our proposed controller reduced energy consumption or the rate of change in required energy after gait transitions compared to before the transitions. Therefore, our method automatically selected the energy-efficient gait, which may allow humanoid robots to achieve more efficient motion behavior.

Our mechanical model, to account for the relationship between leg length and viscoelasticity, exhibits qualitatively similar characteristics to the human leg. The human leg is a linkage mechanism that reaches a singularity at the end of its extension and is driven by muscles with viscoelastic elements. In this structure, the change rate of the knee joint angle in relation to leg length varies, resulting in different mechanical behaviors depending on its length. Consequently, viscous forces dominate when the leg is extended, yielding a rigid leg akin to the IP model. In contrast, elastic forces prevail when the leg is contracted, resulting in a compliant leg akin to the SLIP model. Similarly, our model transitions between elasticity and inelasticity based on leg length, suggesting that even with a linkage structure

https://doi.org/10.1017/S0263574724002248 Published online by Cambridge University Press

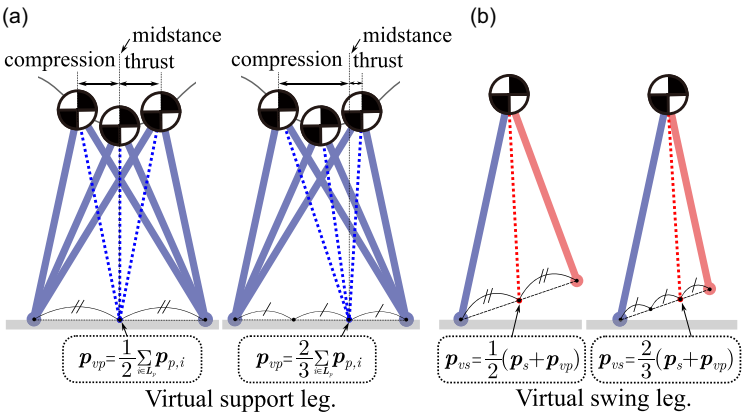


Figure 9. *Behavior of different virtual leg parameters. Panel(a) shows the behavior of the DS phase when the coefficient of (6) is varied. Panel(b) shows the behavior of the free leg when the coefficient of (7) is varied.*

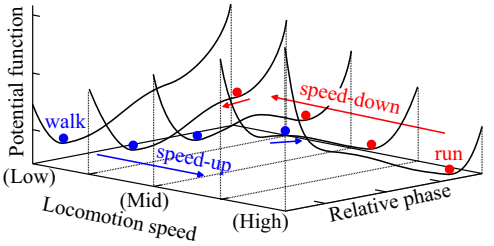


Figure 10. *An assumed potential function that explains the hysteresis in the gait transition (modified from [4, 12]).*

similar to humans, it can naturally exhibit both the IP model for walking and the SLIP model for running, depending on the locomotion speed.

Our state model employs the virtual legs to commonly represent running and walking. The behavior of the virtual legs changes depending on the coefficients applied to (6) and (7) as shown in Figure 9. As shown in panel (a), modifying the coefficient of (6) alters the midstance posture and the timing of the kick (thrust phase). Similarly, modifying the coefficient of (7), as illustrated in panel (b), changes the point of the swing leg and, consequently, the stride length at touchdown. The model assumes uniform physical parameters for all actual legs, with the trajectories of the support legs being symmetrical around the midstance position at a steady state. In animals, the stiffness and natural leg length can differ between legs [32], potentially resulting in asymmetrical supporting leg motion. By adjusting the parameters of the virtual legs, it may be possible to achieve control that accommodates these asymmetrical support leg trajectories.

The results of two simulations representing gait transitions indicate that transitions occur at different speeds. The velocity range for gait transitions during deceleration is smaller than during acceleration. Hence, the potential function representing the stability of the locomotion in this simulation could be visualized as shown in Figure 10. In both low and high-speed ranges, only a single attractor is present. When the locomotion converges to one of these attractors, the gait type becomes running at high speeds or walking at low speeds. On the other hand, in the mid-speed range, two attractors exist, leading to hysteresis within the speed range of gait transition. Depending on the direction of the speed change, the same speed can result in running or walking. This phenomenon also occurs in the gait transitions

https://doi.org/10.1017/S0263574724002248 Published online by Cambridge University Press

of animals and aligns with numerous studies [4, 5, 12] showing that gait transitions occur at different speeds based on the direction of speed change.

7. Conclusion

In this study, we aimed to develop a control method that enables passive and adaptive gait transitions by merely setting a target speed without explicitly instructing the gait types. To this end, a bipedal robot model was developed, focusing on the dynamics of the human leg during walking and running. The model consists of a mechanical model that transitions between elastic legs (SLIP model) and inelastic legs (IP model) based on external force and a state model with virtual leg representations that commonly express walking and running. A simple controller, independent of the gait state, was developed using our bipedal robot model. As a result, dynamics simulation showed stable walking and running, demonstrating passive gait transitions in response to locomotion speed. Moreover, the results indicated that the robot adaptively selects a gait suitable for energy efficiency and locomotion speed. These two results indicate that our proposed bipedal robot model possesses the characteristics of both the IP and SLIP models and can adaptively transit an energy-efficient gait depending on the speed. Furthermore, these results support the universal biological insight into the dependency of gait transitions on speed, which occur dependent on speed and lead to efficient locomotion [2, 12, 28, 35]. For future study, a three-dimensional extension with a model incorporating both the torso and legs is necessary for application to real robots. This will contribute to research on adaptive and efficient control of bipedal locomotion robots.

Author contributions. HS and SI conceived and designed the study. HS conducted and developed a controller, simulator, data gathering, and analyses. HS and SI wrote the article.

Financial support. This research received no specific grant from any funding agency, commercial, or not-for-profit sectors.

Competing interests. The authors declare no conflicts of interest exist.

Ethical approval. None.

Supplementary material. The supplementary material for this article can be found at https://doi.org/10.1017/S0263574724002248.

References

[1] R. M. Alexander, "Mechanics of Bipedal Locomotion," **In:** *Zoology*, (Elsevier, 1976) pp. 493–504.
[2] R. M. Alexander, "Optimization and gaits in the locomotion of vertebrates," *Physiol Rev.* **69**(4), 1199–1227 (1989).
[3] M. Anand, J. Seipel and S. Rietdyk, "A modelling approach to the dynamics of gait initiation," *J. R. Soc. Interface* **14**(128), 20170043 (2017).
[4] S. Aoi, D. Katayama, S. Fujiki, N. Tomita, T. Funato, T. Yamashita, K. Senda and K. Tsuchiya, "A stability-based mechanism for hysteresis in the walk–trot transition in quadruped locomotion," *J. R. Soc. Interface* **10**(81), 20120908 (2013).
[5] S. Aoi, T. Yamashita, A. Ichikawa and K. Tsuchiya, "Hysteresis in gait transition induced by changing waist joint stiffness of a quadruped robot driven by nonlinear oscillators with phase resetting," **In:** *IEEE/RSJ International Conference on Intelligent Robots and Systems*, (2010) pp. 1915–1920.
[6] P. A. Bhounsule, "Control of a compass gait walker based on energy regulation using ankle push-off and foot placement," *Robotica* **33**(6), 1314–1324 (2015).
[7] R. Blickhan, "The spring-mass model for running and hopping," *J. Biomech.* **22**(11-12), 1217–1227 (1989).
[8] G. Cavagna, F. Saibene and R. Margaria, "Mechanical work in running," *J. Appl. Physiol.* **19**(2), 249–256 (1964).
[9] B. Dadashzadeh and C. J. Macnab, "Slip-based control of bipedal walking based on two-level control strategy," *Robotica* **38**(8), 1434–1449 (2020).
[10] A. Davoodi, O. Mohseni, A. Seyfarth and M. A. Sharbafi, "From template to anchors: Transfer of virtual pendulum posture control balance template to adaptive neuromuscular gait model increases walking stability," *Roy. Soc. Open Sci.* **6**(3), 181911 (2019).

https://doi.org/10.1017/S0263574724002248 Published online by Cambridge University Press

[11] M. H. Dickinson, C. T. Farley, R. J. Full, M. Koehl, R. Kram and S. Lehman, "How animals move: An integrative view," *Science* **288**(5463), 100–106 (2000).

[12] F. J. Diedrich and W. H. Warren Jr, "Why change gaits? dynamics of the walk-run transition," *J. Exp. Psychol. Hum. Percept. Perform.* **21**(1), 183–202 (1995).

[13] J. Ding, T. Y. Moore and Z. Gan, "A template model explains jerboa gait transitions across a broad range of speeds," *Front. Bioeng. Biotechnol.* **10**, 804826 (2022).

[14] T. Egle, J. Englsberger and C. Ott, "Analytical center of mass trajectory generation for humanoid walking and running with continuous gait transitions," **In:** *IEEE-RAS International Conference on Humanoid Robots*, (2022) pp. 630–637.

[15] H. Geyer, U. Saranli, A. Goswami and P. Vadakkepat, "Gait Based On the Spring-Loaded Inverted Pendulum," **In:** *Humanoid Robotics: A Reference*, (Springer, Netherlands, 2018) pp. 1–25.

[16] H. Geyer, A. Seyfarth and R. Blickhan, "Compliant leg behaviour explains basic dynamics of walking and running," *Proc. R. Soc. B: Biol. Sci.* **273**(1603), 2861–2867 (2006).

[17] B. Han, X. Luo, Q. Liu, B. Zhou and X. Chen, "Hybrid control for slip-based robots running on unknown rough terrain," *Robotica* **32**(7), 1065–1080 (2014).

[18] S. Hanasaki, Y. Tazaki, H. Nagano and Y. Yokokohji, "Running trajectory generation including gait transition between walking based on the time-varying linear inverted pendulum mode," **In:** *IEEE-RAS International Conference on Humanoid Robots*, (IEEE, 2022) pp. 851–857.

[19] J. K. Hodgins, "Biped gait transitions," **In:** *IEEE International Conference on Robotics and Automation*, (1991) pp. 2092–2097.

[20] D. F. Hoyt and C. R. Taylor, "Gait and the energetics of locomotion in horses," *Nature* **292**(5820), 239–240 (1981).

[21] S. Jana and A. Gupta, "Walking and jogging at similar speeds with a passive slip model based compliant biped," *J. Biomech. Sci. Eng.* **19**(4), 24-00158–24-00158 (2024).

[22] W. Ju, B. Li, R. Kang, S. Zhang and Z. Song, "Design of a torsional compliant mechanism with given discrete torque-deflection points for nonlinear stiffness elastic actuator," *Robotica* **41**(9), 2571–2587 (2023).

[23] S. Kajita, F. Kanehiro, K. Kaneko, K. Fujiwara, K. Harada, K. Yokoi and H. Hirukawa, "Biped walking pattern generation by using preview control of zero-moment point," **In:** *IEEE International Conference on Robotics and Automation*, (IEEE, Vol. **2**, 2003) pp. 1620–1626.

[24] T. Kamioka, H. Kaneko, M. Kuroda, C. Tanaka, S. Shirokura, M. Takeda and T. Yoshiike, "Push recovery strategy of dynamic gait transition between walking, running and hopping," *Int. J. Hum. Robot.* **16**(03), 1940001 (2019).

[25] M. S. Khan and R. K. Mandava, "A review on gait generation of the biped robot on various terrains," *Robotica* **41**(6), 1888–1930 (2023).

[26] T. Kobayashi, K. Sekiyama, Y. Hasegawa, T. Aoyama and T. Fukuda, "Unified bipedal gait for autonomous transition between walking and running in pursuit of energy minimization," *Robot. Auton. Syst.* **103**, 27–41 (2018).

[27] I. M. Koo, T. D. Trong, Y. H. Lee, H. Moon, J. Koo, S. Park and H. R. Choi, "Biologically inspired gait transition control for a quadruped walking robot," *Auton. Robot.* **39**(2), 169–182 (2015).

[28] R. Kram, A. Domingo and D. P. Ferris, "Effect of reduced gravity on the preferred walk-run transition speed," *J. Exp. Biol.* **200**(4), 821–826 (1997).

[29] A. D. Kuo, "The six determinants of gait and the inverted pendulum analogy: A dynamic walking perspective," *Hum. Movement Sci.* **26**(4), 617–656 (2007).

[30] A. D. Kuo, J. M. Donelan and A. Ruina, "Energetic consequences of walking like an inverted pendulum: Step-to-step transitions," *Exerc. Sport Sci. Rev.* **33**(2), 88–97 (2005).

[31] O. Kwon and J. H. Park, "Gait transitions for walking and running of biped robots," **In:** *IEEE international conference on robotics and automation*, (IEEE, Vol. **1**, 2003) pp. 1350–1355.

[32] T. Ma, J. Zhu, K. Zhang, W. Xiao, H. Liu, Y. Leng, H. Yu and C. Fu, "Gait phase subdivision and leg stiffness estimation during stair climbing," *IEEE T. Neur. Sys. Reh.* **30**, 860–868 (2022).

[33] T. A. McMahon and G. C. Cheng, "The mechanics of running: How does stiffness couple with speed?," *J. Biomech.* **23**(Suppl 1), 65–78 (1990).

[34] G. Mesesan, R. Schuller, J. Englsberger, C. Ott and A. Albu-Schäffer, "Unified motion planner for walking, running, and jumping using the three-dimensional divergent component of motion," *IEEE T. Robot.* **39**(6), 4443–4463 (2023).

[35] A. E. Minetti, "Biomechanics: Walking on other planets," *Nature* **409**(6819), 467–469 (2001).

[36] D. E. Orin, A. Goswami and S.-H. Lee, "Centroidal dynamics of a humanoid robot," *Auton. Robot.* **35**(2-3), 161–176 (2013).

[37] D. Owaki, K. Osuka and A. Ishiguro, "Gait transition between passive dynamic walking and running by changing the body elasticity," **In:** *SICE Annual Conference*, (IEEE, 2008) pp. 2513–2518.

[38] M. H. Raibert. *Legged Robots that Balance* (MIT press, 1986).

[39] S. Rezazadeh and J. W. Hurst, "Control of atrias in three dimensions: Walking as a forced-oscillation problem," *Int. J. Robot. Res.* **39**(7), 774–796 (2020).

[40] C. P. Santos and V. Matos, "Gait transition and modulation in a quadruped robot: A brainstem-like modulation approach," *Robot. Auton. Syst.* **59**(9), 620–634 (2011).

[41] V. Segers, K. De Smet, I. Van Caekenberghe, P. Aerts and D. De Clercq, "Biomechanics of spontaneous overground walk-to-run transition," *J. Exp. Biol.* **216**(16), 3047–3054 (2013).

[42] M. Shahbazi, R. Babuška and G. A. Lopes, "Unified modeling and control of walking and running on the spring-loaded inverted pendulum," *IEEE T. Robot.* **32**(5), 1178–1195 (2016a).

[43] M. Shahbazi, G. Lopes and R. Babuska, "Automated transitions between walking and running in legged robots," *IFAC Proc. Vol.* **47**(3), 2171–2176 (2014).

https://doi.org/10.1017/S0263574724002248 Published online by Cambridge University Press

[44] M. Shahbazi, U. Saranlı, R. Babuška and G. A. Lopes, "Approximate analytical solutions to the double-stance dynamics of the lossy spring-loaded inverted pendulum," *Bioinspir. Biomim.* **12**(1), 016003 (2016b).
[45] F. M. Smaldone, N. Scianca, L. Lanari and G. Oriolo, "From walking to running: 3d humanoid gait generation via mpc," *Frontiers in Robotics and AI* **9**, 876613 (2022).
[46] T. Sugihara, "Standing stabilizability and stepping maneuver in planar bipedalism based on the best com-zmp regulator," **In:** *IEEE International Conference on Robotics and Automation*, (IEEE, 2009) pp. 1966–1971.
[47] T. Sugihara and M. Morisawa, "A survey: Dynamics of humanoid robots," *Adv. Robotics* **34**(21-22), 1338–1352 (2020).
[48] G. Taga, Y. Yamaguchi and H. Shimizu, "Self-organized control of bipedal locomotion by neural oscillators in unpredictable environment," *Biol. Cybern.* **65**(3), 147–159 (1991).
[49] T. Takenaka, T. Matsumoto and T. Yoshiike, "Real time motion generation and control for biped robot-1 st report: Walking gait pattern generation," **In:** *IEEE/RSJ International Conference on Intelligent Robots and Systems*, (IEEE, 2009) pp. 1084–1091.
[50] E. V. Vasudevan, S. K. Patrick and J. F. Yang, "Gait transitions in human infants: Coping with extremes of treadmill speed," *PLoS One* **11**(2), e0148124 (2016).
[51] M. Voigt and E. A. Hansen, "The puzzle of the walk-to-run transition in humans," *Gait Posture* **86**, 319–326 (2021).
[52] M. Vukobratović and B. Borovac, "Zero-moment point–thirty five years of its life," *Int. J. Hum. Robot.* **1**(01), 157–173 (2004).
[53] B. Wang, K. Zhang, X. Ma and L. Jia, "A compliant leg design combining pantograph structure with leaf springs," *Robotica* **42**(2), 332–346 (2024).

Cite this article: H. Shin and S. Ikemoto (2025). "A simple bipedal robot model demonstrating speed-dependent gait transition", Robotica **43**, 868–886. https://doi.org/10.1017/S0263574724002248

https://doi.org/10.1017/S0263574724002248 Published online by Cambridge University Press